

Programmed-triboelectric nanogenerators—A multi-switch regulation methodology for energy manipulation

Hao Wang^{a,b,c,d,*}, Jianxiong Zhu^{a,b,c,1}, Tianyiyi He^{a,b,c}, Zixuan Zhang^{a,b,c},
Chengkuo Lee^{a,b,c,e,**}

^a Department of Electrical and Computer Engineering, National University of Singapore, Singapore

^b Center for Intelligent Sensors and MEMS (CISM), National University of Singapore, Singapore

^c NUS Suzhou Research Institute (NUSRI), Suzhou, China

^d Institute of Biomedical & Health Engineering, Shenzhen Institute of Advanced Technology (SIAT), Chinese Academy of Sciences (CAS), Shenzhen, 518035, China

^e NUS Graduate School for Integrative Science and Engineering (NGS), National University of Singapore, Singapore

ARTICLE INFO

Keywords:

Programmed-triboelectric nanogenerators
Multi-switch regulation methodology
Bennet doubler
Charge manipulation
Output amplification
Breakdown

ABSTRACT

Energy manipulation from the mechanical power source is an essential segment for self-powered electronics and the potential application in the Internet of Things. Inspired by the concept of programming, we proposed a programmed-triboelectric nanogenerators (P-TENGs) using mechanical switches regulation methodology for energy manipulation. It is based on three unit-operations, which were extracted from the mechanism of conventional TENGs. A specific sequence and combination of the three unit-operations, considered as a program realized by hardware, can achieve a power amplification easily, which is desired for the design of TENGs devices. There can be an infinite number of feasible programs to be designed based on the specific application scenarios and physical constraints. In this study, three different programs, current amplifier, Bennet doubler, and charge oscillator, are designed and physically realized to illustrate the programming concept and achieve a ~kV level voltage output. The material selection and structure design, which is the major concern for conventional TENGs devices, no longer exist in P-TENGs. Even the contact surfaces with the same material still make the device functional. Instead, P-TENGs meet other constraints such as high-k coating materials and high voltage breakdown. It is envisioned that the proposed mechanical switches regulation methodology can enable an alternative approach to the research of triboelectric nanogenerators.

1. Introduction

Since firstly developed by Zhonglin Wang [1–5], the triboelectric nanogenerators (TENGs) has demonstrated its promising capability on energy harvesting from various kinds of sources and universal adaptability on all kinds of physical and chemical sensing scenarios [6–34]. Up to now, the major improvement of the TENGs devices, either for energy harvesting or self-powered sensing, is based on the optimization of the materials and the design of the structures [35–84,97,98]. No matter how the material and structure changes, the basic working principle of the TENGs devices remains the same: a specific physical operation, which can be either contact-separation or sliding, to induce electrostatic charge by friction and further generates power upon the

load. Two independent physical procedures happen in this basic working principle: charge generation by friction and power generation by the capacitance change of the device. Although conventionally, these two procedures are mixed in the operation of the TENGs devices, we are still able to design and optimize them in the device level separately.

Along with the charge accumulation to power electronic device, one of the worthwhile trials is introducing the concept of the charge pump, which is a plate enabling a charge accumulation [85–90]. TENGs can leverage the accumulated charges on this plate via either some particular circuit, such as a Bennet doubler conditioning circuit [85–88,91–96,99], or another TENGs device, which means charging one TENGs by another [89,90]. Based on this idea, the charge generated on the TENGs device is not only from itself but also enhanced by some external parts,

* Corresponding author. Department of Electrical and Computer Engineering, National University of Singapore, Singapore.

** Corresponding author. Department of Electrical and Computer Engineering, National University of Singapore, Singapore.

E-mail addresses: hao.wang@siat.ac.cn (H. Wang), elelc@nus.edu.sg (C. Lee).

¹ Hao Wang and Jianxiong Zhu contributed equally to this work.

which can be either a circuit or a physical device. To further analyze the fully disassembled working principle of the TENGs, three fundamental operations, called unit-operations, were summarized. A new strategy by programming the sequence of the unit-operations, instead of optimizing materials and external electronics units, is proposed for boosting the output of TENGs. It is called programmed-triboelectric nanogenerators (P-TENGs). The three unit-operations can be arbitrarily programmed with a specific sequence and combination to realize an exact function: power amplification. Rather than optimizing the material and structure, the design of TENGs more like writing a program. As a computer program realized by switching operations of transistors, we introduced a similar switching concept to manipulate the charge flow in the operation of TENGs for realizing a specific function for an infinite number of possible programs to design. To demonstrate our proposed strategy for energy manipulation, three different programs, which called current amplifier, Bennet doubler, and charge oscillator, are designed and physically realized to illustrate the programming concept and achieve a ~kV level voltage output. The material selection and structure design, which is the major concern for conventional TENGs devices, no longer exist in P-TENGs. Even the contact surfaces with the same material still make the device functional. It is a step by step guide for readers to master the idea of the P-TENGs in terms of program design, physical realization, and performance characterization. It also envisions that the proposed mechanical switches regulation methodology can enable an alternative approach to the research of triboelectric nanogenerators for energy manipulation.

2. Results and discussion

2.1. Programmed-triboelectric nanogenerators

The concept of P-TENGs is based on three unit-operations in Fig. 1A and B. These three unit-operations can achieve the functions of charge generation, charge transfer, and power output. The detailed mechanisms

of these operations are explained below. Each operation consists of electrode operations and switches operations with time sequence. The electrode operation comprises the contact and separation of two electrodes. The switch operation comprises the on and off connections as follows three phases: the first is charge generation (Fig. 1B-a)-Operation G. There are some initial charges on electrode A. This initial charge can be generated by either friction with other materials or electrostatic induction. This electrode A can be either a dielectric or a metal electrode with a dielectric coating. Then make the electrode A contact with the electrode B and close the switch to make B grounded. Because of the electrostatic induction, electrode B will be charged with identical charge quantity but opposite polarity as the electrode A. Disconnect the switch first and separate electrode A and B, the charge on the electrode B can be kept on it. As seen, this operation enables an electrode to be charged by borrowing charges from the ground. The second phrase is charge transfer (Fig. 1B-b) Operation T. Assume there are charges on both electrodes B and C when they are not connected. Make electrode A contact with electrode B first. Then close both switches to make A grounded and B and C connected. Since electrode A and B form a capacitor, all charges will be accumulated at the interface between them. The charges on electrode C will be transferred onto the electrode B. Meanwhile, the electrode A will be charge with identical charge quantity but opposite polarity as the electrode B. As seen, the major function of this operation is to concentrate charges from multiple electrodes to one electrode. The third phase is called power output (Fig. 1B and c) Operation O. Based on the charge transfer operation, we can achieve an electrode with concentrated charges from multiple electrodes, which is the electrode B. When the electrode A contacts and separates with the electrode B, there is a charge flow on electrode A, which is similar to the charge generation operation. The only difference here is the load connected in series with the electrode A. The charge flow through the load can generate power, which is an energy harvesting process. The function of this energy harvesting operation is to convert the mechanical energy to electric energy by leveraging the accumulated

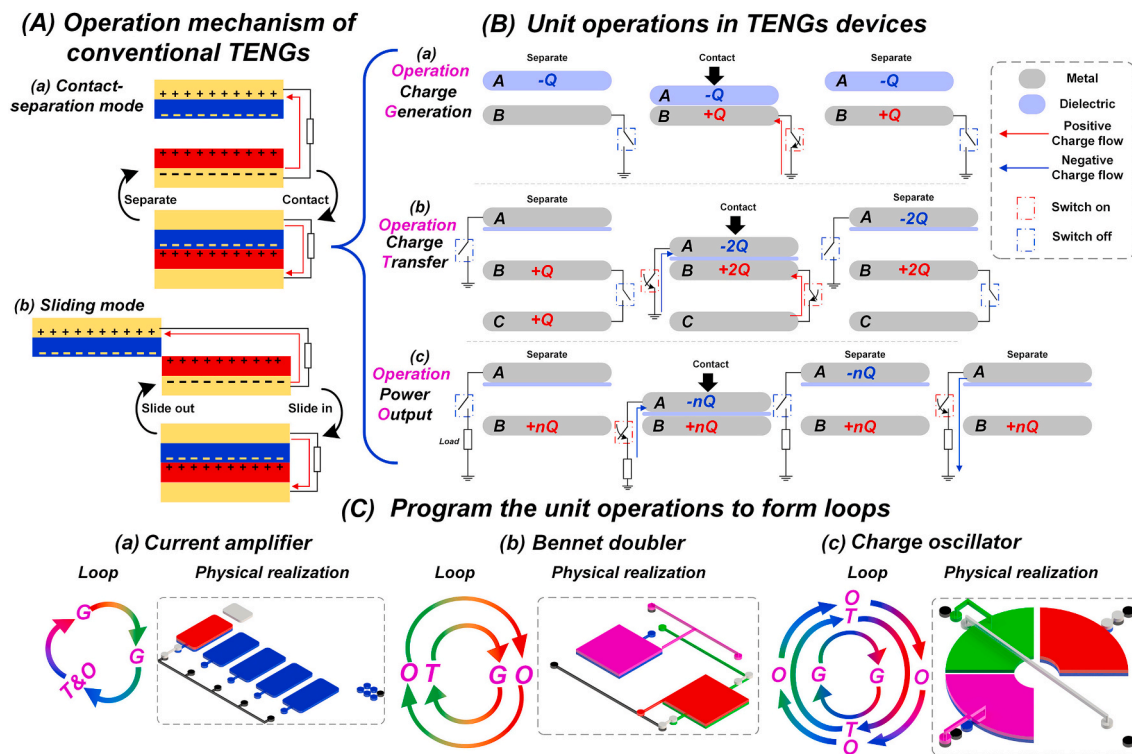


Fig. 1. Concept of programmed TENGs (P-TENGs). (A) The operation mechanism of the conventional TENGs: a, Contact-separation mode; b, Sliding mode; (B) The three unit-operations to be extracted from the mechanism of TENGs: a, Operation G: charge generation; b, Operation T: charge transfer; c, Operation O: power output; (C) Feasible programs to be realized in this study: a, Current amplifier; b, Bennet doubler; c, Charge oscillator.

charge on electrode **B**.

As seen, just like programming software, charges can be arbitrarily operated by a specific combination and sequence of the three operations (G, T, and O) for a specific purpose, e.g., amplifying the. Therefore, such a specific operation combination of charge manipulation is considered as a program, which is realized by hardware rather than software. Then the three basic operations are equivalent to the basic codes in software. Thus, designing a TENGs is more like writing a program rather than developing new structures and optimizing material selections, which is the main concern for conventional TENGs devices. There are some principles and constraints for designing a P-TENGs. To realize the program in physical, the electrodes can only be operated either out-of-plane (contact-separation) or in-plane (sliding). Meanwhile, the number of electrodes involved in the program is always limited. The program should always form a loop to enable an infinite running. The loop is the most critical factor in determining its physical realization, and the loop can be started from any state and not affected by the initial value. There

are infinite possible programs that can be designed to achieve the function of the output amplification of TENGs. In this study, we will demonstrate several cases as shown in Fig. 1C, from simple to complex, to systematically illustrate how P-TENGs are designed and realized. The purpose of these case demonstrations is not only to show the capability and performance of P-TENGs but more importantly, to promote the concept the programming, which is an alternative direction for the study of triboelectric energy harvesters.

2.2. Current amplifier device of P-TENGs

For conventional TENGs devices, the output current is normally proportional to the area of the contact surfaces. Meanwhile, the TENGs device normally follows the symmetric configuration, in which the top and bottom electrodes are of the same area. Therefore, those devices with sliding mode require a large operation area to achieve enough power output. Based on the concept of P-TENGs, we can design an

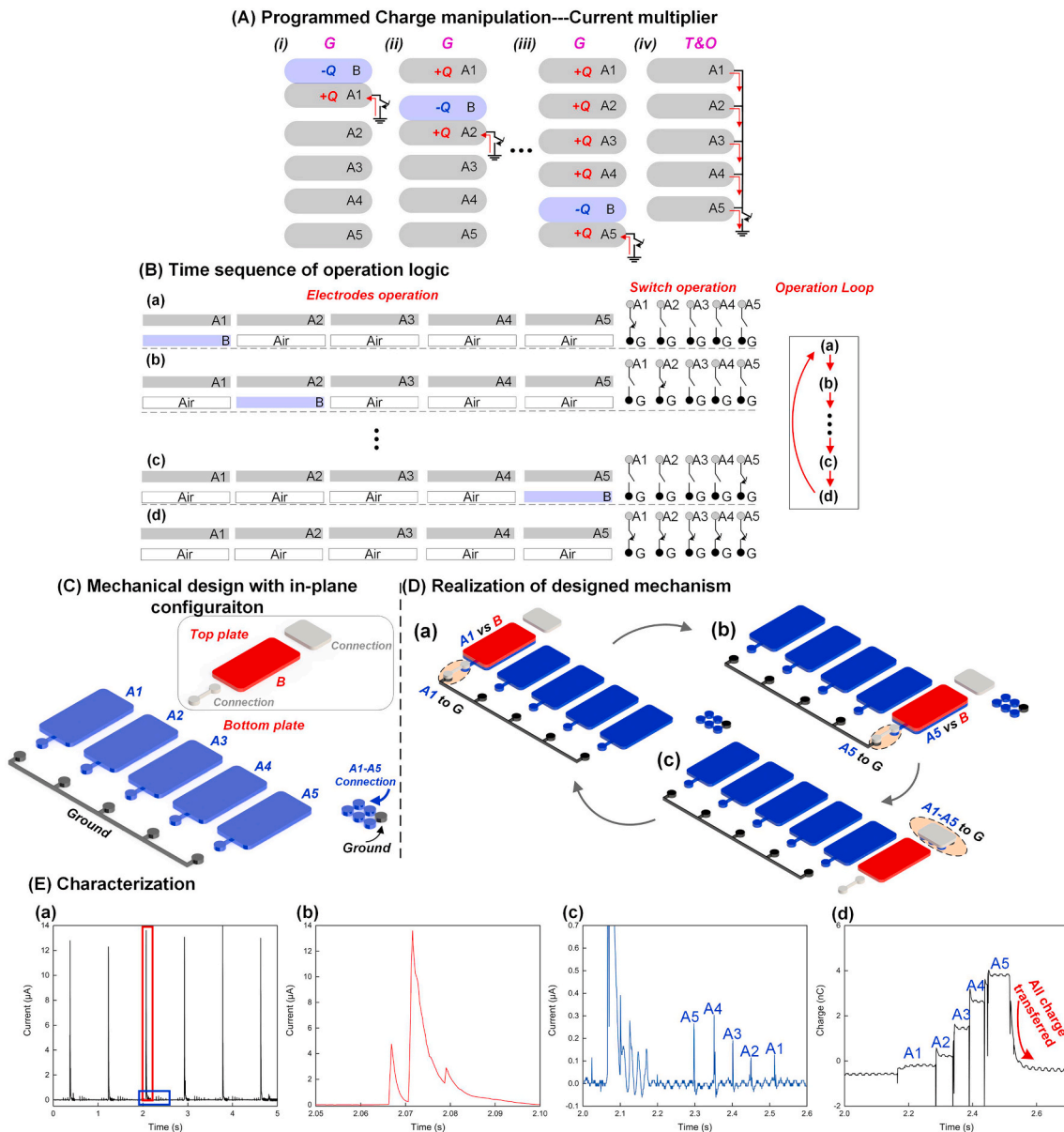


Fig. 2. The design of the current amplifier. (A) The program of the charge manipulation; (B) The time sequence and operation logic of all the electrodes, switches and the loop form; (C) The mechanical design with in-plane configuration; (D) Realization of the designed mechanism; (E) The characterization of the current amplifier: a, the short circuit current; b, the detailed waveform of the amplified current peak; c, The detailed waveform of charging each electrode when electrode **B** is sliding; d, the charge curve of the sliding operation. The load resistance for the measurement of current is 100MΩ.

asymmetric TENGs device, in which the top electrode is small while the bottom electrode is large, to generate a large current as a large area device with a small sliding electrode. It is called the current amplifier.

Designing a P-TENGs always starts with programming the charge manipulation. This current amplifier is a simple case to demonstrate how the three basic operations are coded in one program to achieve an output amplification. The detailed program is shown in Fig. 2A. There are six plates and five switches involved in this program. The electrode B is a pure dielectric plate, while others are metal electrodes. The electrode B generates charges by operation G on all the five electrodes. Then at the last step of one cycle, all the electrodes are connected and grounded simultaneously. At this instant, all the charges accumulated on five electrodes can be transferred together (operation T and O), forming a much-amplified current flow. The second step of designing a P-TENGs is to analyze the detailed operation sequence of all the electrodes and switches and to figure out the loop form. This step helps make clear how many switches are required and how to arrange all the electrodes. As shown in Fig. 2B, the situation of each electrode (contact with which electrode) and switch (on or off) is listed here. When an electrode faces no other electrode, it is defined as facing the air. This loop of the whole operation is circular. This program can be easily realized with an in-plane sliding structure made by acrylic plates, as shown in Fig. 2C. There are two plates required: top and bottom plates. The electrode B,

which is a dielectric layer, is arranged on the top plate. All the other electrodes, A1 to A5, are on the bottom plate. Meanwhile, there are switch pads to be arranged on both top and bottom plates to realize all switch operations during the sliding operation. The detailed physical operation is illustrated in Fig. 2D. The electrode B contacts with A1 and A1 is grounded (Fig. 2D-a). Then the top plate slides from A1 to A5, generating charges on each electrode (Fig. 2D-b). Further, slide the top plate to make the connection pad contact with all the switch pads of A1 to A5 and the ground (Fig. 2D-c). The optical image of the device is shown in Supplementary S1 and the operation can be seen in Supplementary video V1. The wiring information of the current amplifier is shown in Supplementary Figure S1.1.

Supplementary video related to this article can be found at <https://doi.org/10.1016/j.nanoen.2020.105241>

To demonstrate the characterization of the current amplifier-based P-TENGs, the major function of this P-TENGs is to amplify the current and charge output, as characterized in Fig. 2E. The curve of the short circuit current in Fig. 2E-a shows the major peaks, which are the amplified current, can be up to about 13 μ A. The detailed current waveform of the major peak is shown in Fig. 2E-b. As seen, there can be a breakdown between the electrode pads before they fully contact each other, so there is more than one exponential peak to be observed. There are minor current peaks generated by charging the electrodes A1 to A5,

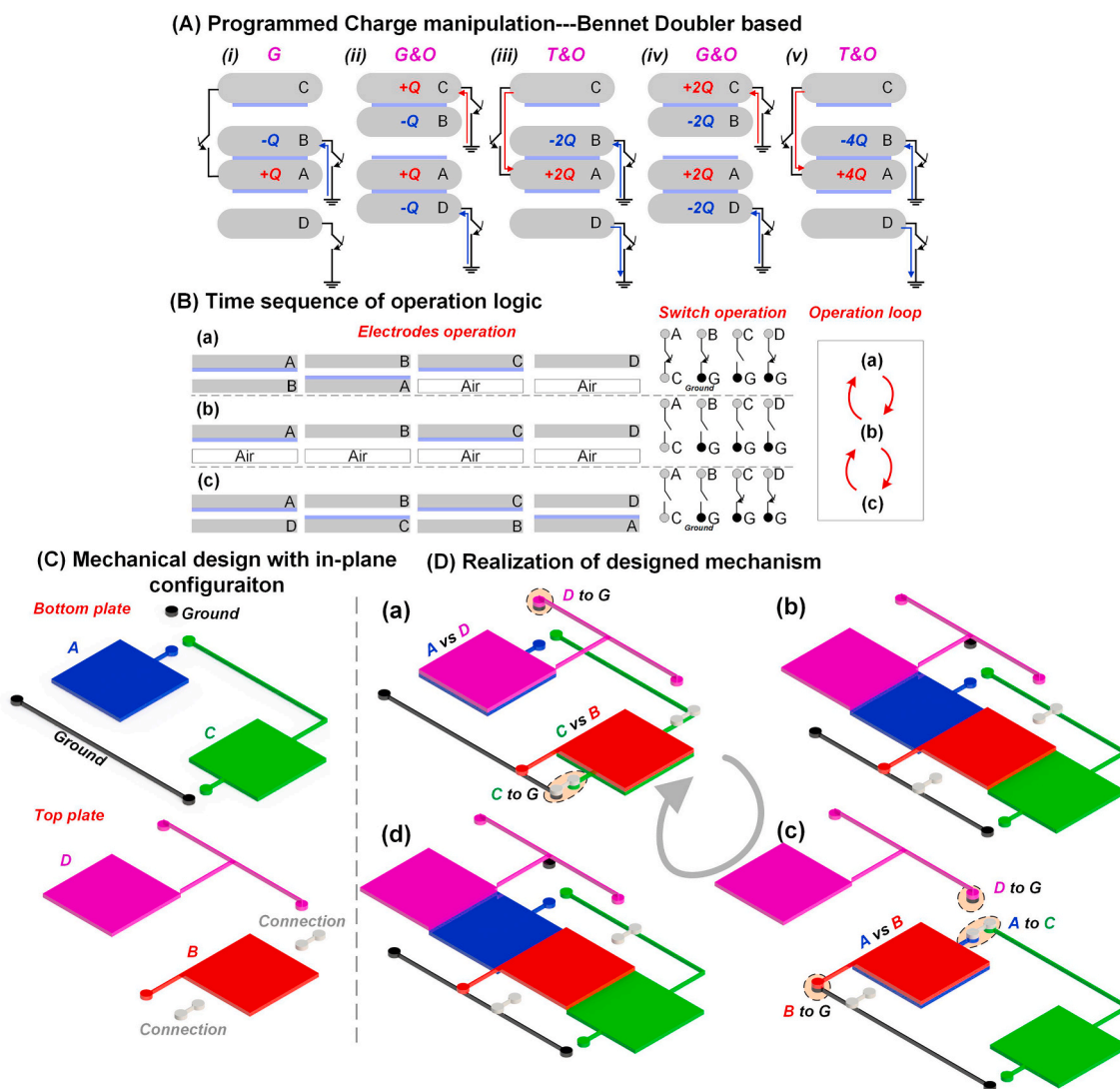


Fig. 3. The design of the in-plane Bennet doubler-based P-TENGs. (A) The program of the charge manipulation; (B) The time sequence and operation logic of all the electrodes, switches, and the loop form; (C) The mechanical design with the in-plane configuration; (D) Realization of designed mechanism.

between two major current peaks. The detailed waveform is shown in Fig. 2E-c. Since there are five electrodes to be charged during the operation, five minor current peaks are observed in the curve. As seen, none minor current peak is higher than $0.3 \mu\text{A}$ while the final amplified major peak can be $13 \mu\text{A}$. The charge output curve in Fig. 2E-d shows how charges are generated on each electrode and transferred together at the last step. From this characterization, it is confirmed that the programmed charge manipulation can be realized with a proper mechanical design.

2.3. Bennet doubler device in-plane design in P-TENGs

Bennet doubler is a clever device for the continuous doubling of a small initial charge through a sequence of operations with three electrodes. It was invented in 1787 by the Reverend Abraham Bennet, that used it for studies about the electric state of the air. The original version of the Bennet doubler only has three electrodes (A, B and C in Fig. 3A). In this study, it was improved by adding an extra electrode D for achieving continuous power output without charge consumption of the whole system. The detailed charge manipulation is shown in Fig. 3A. There are four electrodes involved in this program. The bottom side of the electrode C and both sides of the electrode A are covered with dielectric layers. Assuming there is some initial charge on the electrode A, which is generated by friction. In step (A-i), electrode B is charged by operation G via electrode A. Then, in step (A-ii), electrode C is charged by operation G via electrode B. Electrode A contacts with electrode D for operation O, power output. Then in step (A-iii), A separates from D for another operation O. The charge transfer, operation T, from C to A, is achieved via electrode B. As seen, now the charge on electrode A is doubled (from 1Q to 2Q) compared with step (A-i). Then after another cycle ((A-iv) and (A-v)), the charge on electrode A has doubled again (from 2Q to 4Q). As seen, two adjacent states form a cycle. The key point of the program is that the charge on electrode A can be doubled in each cycle. Thus, this electrode can be considered as a charge pump, where charges can accumulate there. The induced charges on electrode D can increase together with electrode A and achieve an increased energy output. As long as the electrode A never grounded, the charges on it can be kept. There are four electrodes and four switches involved in this program. A detailed analysis of the condition of electrodes and switches is shown in Fig. 3B, which is summarized according to Fig. 3A. The state (B-a) and (B-c) refers to the state (A-i) and (A-ii), respectively. When an electrode faces no other electrodes, it is defined as facing air. Between the state of (B-a) and (B-c), there is an intermediate state, when all electrodes are separated from each other. Thus, in this state, all electrodes are facing air, and all switches are off. There are three possible states in total. The loop form is shown in Fig. 3B (Operation loop). As seen, the system is just dangling between state (a) and (c) via state (b). This situation indicates that, rather than a circular operation, a back and forth operation is more suitable to realize this program physically. Whether to use a back and forth operation or a circular operation depends on the loop form. In the next section, it is shown how a circular operation is necessary to realize another program. Both in-plane and out-of-plane mechanical structures, which are demonstrated in this study, can very easily realize a back and forth operation.

The in-plane design for sliding operation is shown in Fig. 3C. There are two plates required to arrange all the four electrodes and switches. Since electrodes A never touches C and B never touches D, A and C are arranged on the bottom plate while B and D are arranged on the top plate. Each electrode is $7 \times 7 \text{ cm}^2$. There are some extra electrode patterns, called switch electrodes, on plates to realize all the switch operations during the physical sliding automatically. The exact sliding operation is shown in Fig. 3D. At the initial state (Fig. 3D-a), A vs D while B vs C. Then slide the top plate (Fig. 3D-b) to make every electrode faces air, which is the intermediate state in Fig. 3B-b. Further slide the top plate (Fig. 3D-c) to make B vs A. Then slide back the top plate, via state (D-d), to the initial state (Fig. 3D-a). A proper layout of the

switch electrodes can achieve the correct switch operation during the sliding.

Any non-conductive materials can be used as the substrate of the device. In this study, we used acrylic plates, which can be easily patterned by a laser cutter, as the top and bottom plates. The image of the actual device is shown in Fig. S2. The sliding operation with voltage output is shown in Supplementary Video V2. Theoretically, the charge on the electrode A can have an infinite accumulation without limit. However, in the actual testing, there will be a breakdown between operational electrodes when the voltage is higher than a threshold. An illustration of this breakdown is shown in Fig. 4d. During the sliding, the distribution of the charge on the electrode will also change with the relative position of the two electrodes. When the two electrodes are fully overlapped (Fig. 4d-i), the charge can have a relatively uniform distribution. However, when two electrodes are about to separate from each other fully, all charges will be accumulated at the edge and tend to have a breakdown between operational electrodes (Fig. 4d-ii), which is similar to the situation of the tip discharge. The maximum voltage or the maximum charged can be accumulated on the electrode A is determined by how much voltage the dielectric layer can sustain. By changing the materials of the dielectric layer, we can have different maximum voltage. In this study, two materials, Fluorinated ethylene propylene film (FEP) and Polytetrafluoroethylene (PTFE) film, are selected as the dielectric coating. The FEP film and PTFE film are of $220 \mu\text{m}$ and $300 \mu\text{m}$ thickness, respectively. There are two combinations as shown in Fig. 4a, FEP vs FEP ($440 \mu\text{m}$ thickness), and FEP vs PTFE ($740 \mu\text{m}$), are tested. Since the dielectric constant of these two materials is quite close (~ 2.03), so the difference mainly comes from different dielectric thicknesses. Since the operation O is achieved by electrode D, the testing of the energy output is also measured on the load resistance connected in series with the electrode D. There are two possible measurement modes. One is switching mode, which is just the same as shown in Fig. 4D: the switch is closed only at the state (D-a) and (D-c). In this mode, the generated voltage should follow a standard RC discharge waveform, which is exponential. Another is a continuous mode, which means the electrode D is directly connected with the load resistance. In this mode, the generated voltage follows a normal TENGs waveform. Detailed performance characterization of the Bennet doubler-based P-TENGs is shown in Fig. 4. In switching mode, the load resistance value only affects the pulse width of the exponential voltage waveform but does not affect its amplitude. The measured voltage curves for both dielectric combination groups are shown in Fig. 4b. As seen, both curves show a gradually increasing trend with the operation and finally saturated at a certain value. The curve of FEP vs PTFE show a much higher voltage, which is about 1300 V, than that of FEP vs FEP, which is about 800 V. As mentioned above, the FEP vs PTFE has a thicker dielectric layer, which is $740 \mu\text{m}$ so that it can stand a higher breakdown voltage. The voltage cannot have an infinite increase because of the breakdown between operational electrodes. The evidence of this breakdown can be found in the detailed voltage waveform as shown in Fig. 4c. In the switching mode, the voltage should have appeared only at the instance when the switch is connected. However, before the RC voltage waveforms happen, there is another irregular voltage waveform, with a lot of small spikes, indicated as breakdown between switches. Breakdown voltage always has a lot of spikes. This breakdown happens between the switch pads rather than the operation electrodes. Before the switch is about to be connected, the spacing between the two pads is very low, and the breakdown happens through the air. Since this breakdown current shares the same direction as the current after the switch is connected, the polarity of the breakdown voltage is the same as the RC discharge follows it. Another breakdown happens inside the RC discharge waveform, which is the breakdown between operational electrodes explained in Fig. 4d. This breakdown attenuates the shape of the exponential waveform, making it not so regular. Since the breakdown current is opposite to the output current through the load resistance, the spikes of the breakdown voltage are opposite to the RC discharge waveform. The

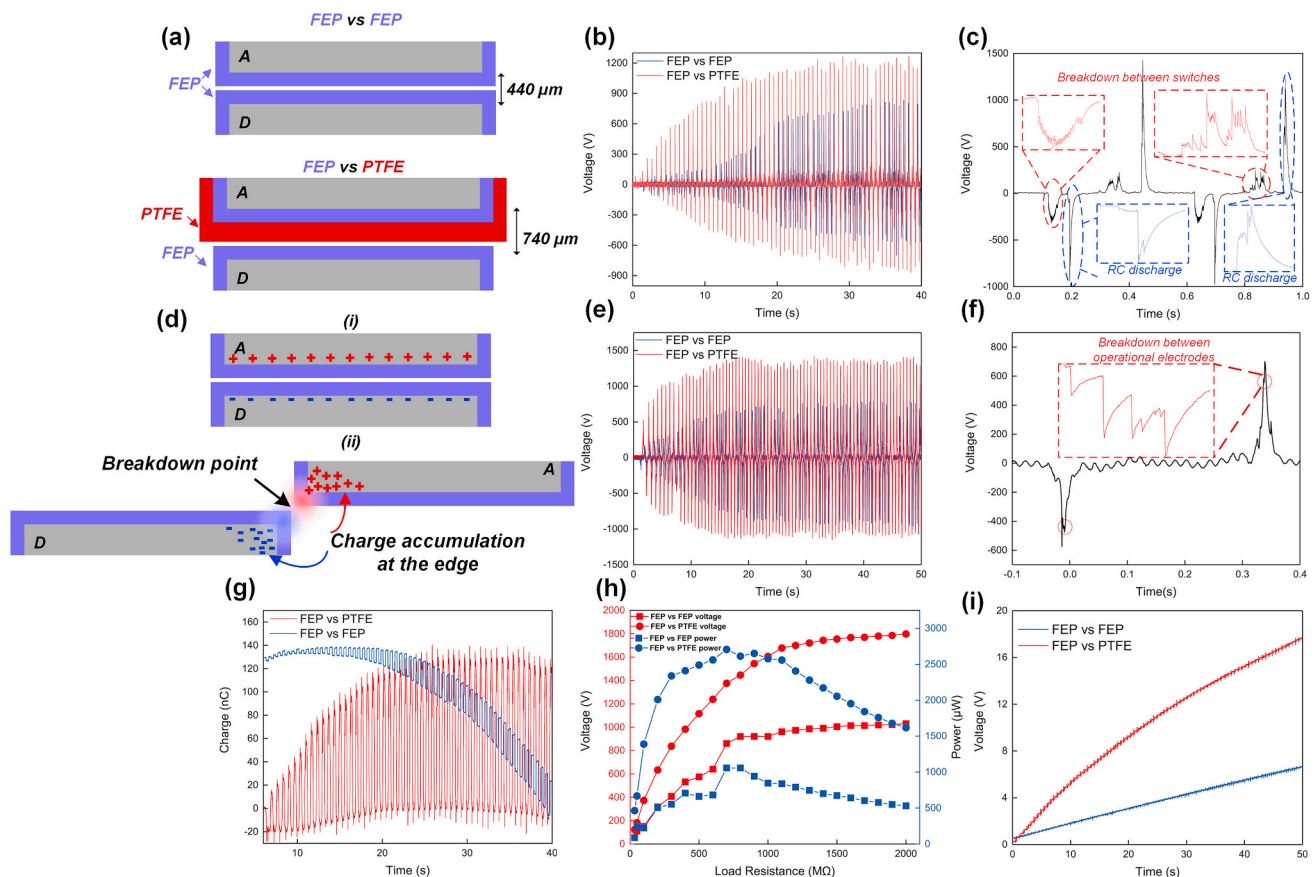


Fig. 4. Characterization of the in-plane design of the Bennet doubler-based P-TENGs. (a) The two dielectric layer combination groups in tests; (b) The output voltage of the two groups in switching mode; (c) The detailed voltage waveforms showing the breakdown spikes; (d) The situation of breakdown happens when two electrodes are not overlapped; (e) The output voltage of the two groups in continuous mode; (f) The detailed voltage waveform showing the breakdown spikes; (g) The charge output of the two groups; (h) The voltage and peak power by changing load resistance; (i) The performance of charging a 0.1 μF capacitor with a full bridge rectifier.

measurement of the output charge is shown in Fig. 4g, showing how the charge output gradually increases from a very small value. Here, the initial charge is generated from friction by either FEP vs FEP or FEP vs PTFE. For the case of FEP vs FEP, since friction surfaces are of the same material, the charge generation efficiency is very low. As seen, the initial charge value is almost zero. However, because of the capability of the P-TENGs to double the charge, the stable charge output can be around 30 nC. For the case of FEP vs PTFE, since the material is different and the dielectric layer is thicker, the charge output reaches a higher stable value, 130 nC, with a shorter duration.

Supplementary video related to this article can be found at <https://doi.org/10.1016/j.nanoen.2020.105241>

In the continuous mode, the output voltage is affected by the load resistance. Fig. 4e shows the voltage curves for both groups with a 700 M Ω load resistor. The same as a result in switching mode, the voltage of FEP vs PTFE, about 1400 V, is higher than that of the FEP vs FEP, which is around 800 V. A detailed voltage sample in Fig. 4f shows that the breakdown between operational electrodes happens when the voltage is approaching the maximum. Meanwhile, since the switch is disabled in this mode, the breakdown between switches, which happens in the switching mode, disappears. A more detailed illustration of the difference between these two breakdowns (between switches and between operational electrodes) is shown in Supplementary Figure S2.2. Fig. 4h shows the characterization of the output voltage and peak power by changing the load resistance. As seen, the maximum voltage by increasing the load resistance can be about 1000 V and 1800 V for the FEP vs FEP and FEP vs PTFE, respectively. The maximum peak power of FEP vs PTFE can be 3 mW at 700 M Ω load, which is 3 times of FEP vs

FEP. The performance of charging a 0.1 μF capacitor is shown in Fig. 4i. With the same operation speed, FEP vs PTFE can charge it to 18 V while FEP vs FEP only achieves 6 V.

2.4. Bennet doubler out-of-plane design in P-TENGs

The out-of-plane design for the contact-separation operation is shown in Fig. 5a. The electrodes B and D are arranged on the left part while electrodes A and C are arranged on the right part. Each electrode is $5 \times 5 \text{ cm}^2$. All the switch pads are arranged on the edges of the parts, shown as the colored round pads. The detailed operation is shown in Fig. 5b. The optical image is shown in Supplementary S3, and the actual operation is shown in Supplementary Video V3. In this out-of-plane design, we only tested the continuous mode (electrode D relates to the load resistance). There are also two different dielectric combination groups, shown in Fig. 5c, were tested. The PTFE vs PTFE is 600 μm thick, and FEP vs PTFE is 520 μm . The voltage curves with a 700 M Ω load resistor is shown in Fig. 5d. As seen, since the friction material is the same for PTFE vs PTFE, the voltage increases slower than that of the FEP vs PTFE. However, due to a thicker dielectric layer, the PTFE vs PTFE has a higher maximum voltage. The short circuit current in Fig. 5e and the output charge in Fig. 5f show the same trend. The characterization for the voltage and peak power is shown in Fig. 5g. The maximum voltage is 1400 V and 1150 V for PTFE vs PTFE and FEP vs PTFE, respectively. Both two groups reach the maximum peak power at around 200 M Ω with 3.3 mW and 2.5 mW, respectively. The performance of charging a 0.1 μF capacitor is shown in Fig. 5h. With the same operation speed, PTFE vs PTFE can charge it to 9.5 V while FEP vs PTFE only achieves 6.5

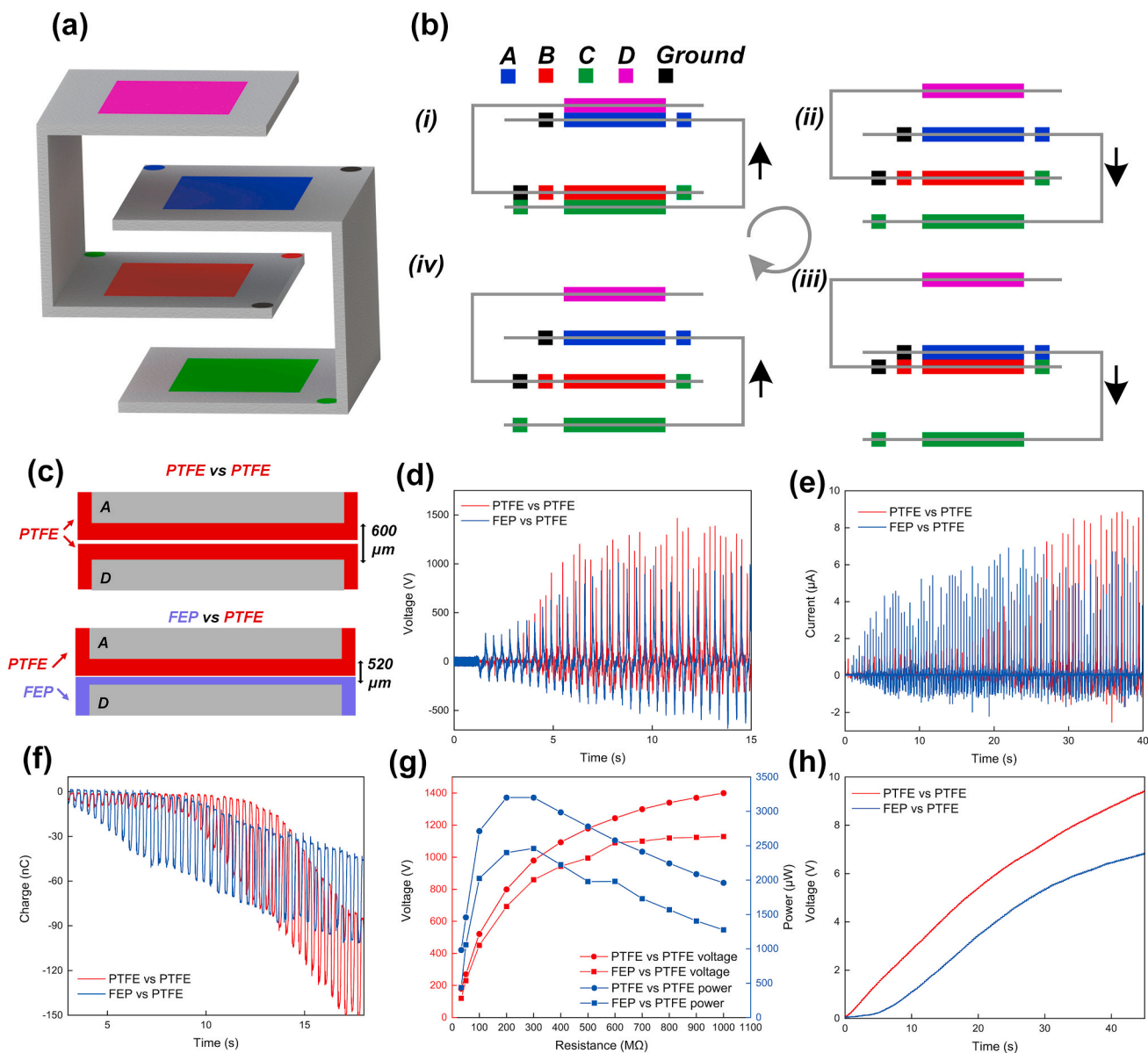


Fig. 5. Characterization of the out-of-plane design of the Bennet doubler-based P-TENGs. (a) The layout design and electrode arrangement of the out-of-plane design; (b) The operation of the out-of-plane design; (c) The two dielectric layer combination groups in tests; (d) The output voltage of two groups in continuous mode with 700 MΩ load resistor; (e) The short circuit current of two groups; (f) The charge output of two groups; (g) The voltage and peak power by changing load resistance; (h) The performance of charging a 0.1 μF capacitor with a full bridge rectifier.

V.

2.5. Charge oscillator in P-TENGs

As mentioned above, based on the concept of programming, there can be an infinite number of possible programs for output amplification. The Bennet doubler, which has been developed for more than 200 years, is just one specific case. Here we designed another program shown in Fig. 6, called charge oscillator, to achieve a similar function. There are five electrodes involved in this program. Among them, the electrode B is purely a dielectric layer. The electrode C and D are covered with a dielectric layer. This electrode B can achieve operation G to generate charges on electrode A1 and A2. The electrode C can achieve operation T to make charges transferred between A1 and A2. The electrode D can achieve operation O to generate power from A1 and A2. This program is called charge oscillator because the charge is oscillating between A1 and A2. The total charge accumulated can have an increment of 2Q in each

cycle. There are five electrodes and five switches involved in this program. The detailed electrode and switch operations are shown in Fig. 6B. There are four states in total, forming a circular loop. Apparently, this circular loop cannot be realized by a back and forth operation. A mechanical structure for rotating operation is inevitable. This program can be realized by two acrylic plates as shown in Fig. 6C. The electrodes A1 and A2 are arranged on the bottom plate while others are arranged on the top plate. Each electrode occupies about one-quarter of the plate. All switch pads are arranged on the edge of the circular plate to realize all switching operations during the rotation. The detailed operation of the device is shown in Fig. 6D. The bottom plate is fixed while the top plate rotates. It is emphasized here that, at state (b) and (d), electrode A1 and A2 are connected via a wire above the plate, which is indicated as “A1 to A2” in the figure. The optical image of the actual device is shown in Supplementary S4. The operation of the device is shown in Supplementary video V4. The dielectric layer of B is FEP (220 μm) and the dielectric layer on electrode C and D is PTFE (300 μm). Since the

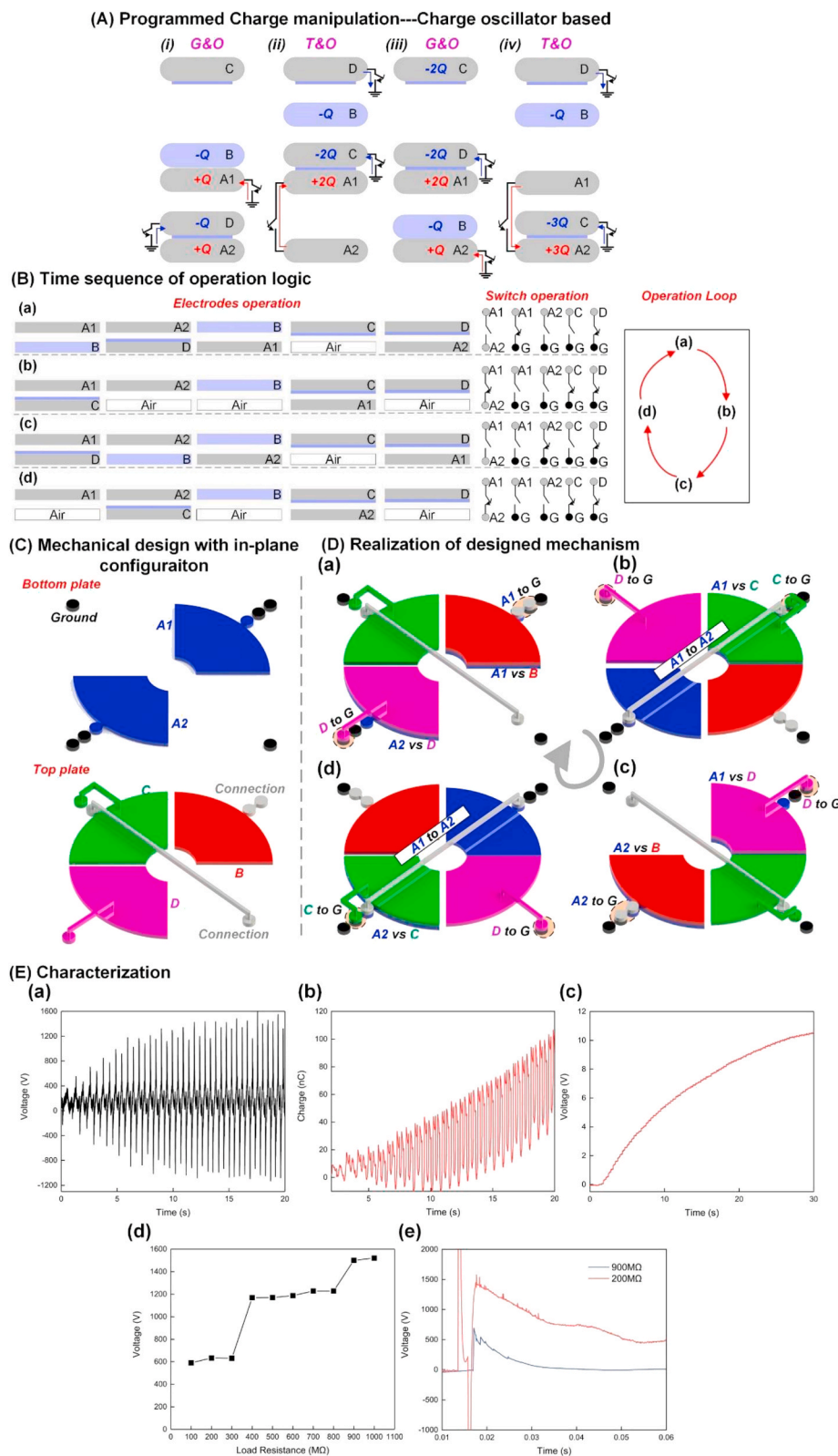


Fig. 6. The design of the Charge oscillator-based P-TENGs. (A) The program of the charge manipulation; (B) The time sequence and operation logic of all the electrodes, switches, and the loop form; (C) The mechanical design with the in-plane configuration; (D) Realization of designed mechanism; (E) Characterization of the Charge oscillator based P-TENGs: a, The output with 1000 MΩ load resistor; b, The charge output; c, The performance of charging a 0.1 μF capacitor with a full bridge rectifier; d, The amplitude of the saturated voltage by changing load resistance; e, The detailed voltage curve of 900 MΩ and 200 MΩ load resistance.

electrode **D**, which is the one for energy output, is on the rotating plate, it is difficult to connect it with a wire for testing directly. It can only be tested in the switching mode via the switch on the plates. A load resistor is connected between the ground and the electrode **D**. The output voltage should follow an RC discharge, which is an exponential waveform. The voltage curve with 1000 MΩ in Fig. 6E-a shows that the

maximum stable voltage can be around 1600 V when the dielectric layer thickness is 520 μm. Considering this dielectric thickness is the same as the one in the out-of-plane Bennet doubler device, so the output voltage also of similar value. The charge output in Fig. 6E-b shows a typical increasing trend and saturates at around 70 nC. This device can charge a 0.1 μF capacitor to 10 V in 30 s, as shown in Fig. 6E-c. Ideally, the

voltage amplitude measured in the switching mode should not vary with the load resistance. However, since the voltage generated by the P-TENG is too high, the breakdown effect plays a dominant role, introducing a complex effect on the measured voltage amplitude as shown in Fig. 6E-d. The actual voltage amplitude can have a step increment by increasing the load resistance. The detailed voltage waveforms at different load resistance (200 M Ω and 900 M Ω) are shown in Fig. 6E-e. As seen, for the curve of 900 M Ω , there is a huge breakdown voltage before the exponential waveform. The amplitude of this breakdown voltage is 2–3 orders higher than the exponential waveform; thus, it cannot be recorded by our system. However, the curve of 200 M Ω does not have this huge breakdown voltage. Instead, the exponential waveform has two peaks. A reasonable explanation is that the discharge happens twice in this curve. One happens when the switch has not been fully connected. The high voltage between the switch pads generates a plasma discharge, forming the first peak and consuming part of the energy. Then before the end of plasma discharge, the switch is connected, forming the second peak. Since the total energy is divided into these two discharging processes, the measured voltage amplitude decreases. After introducing all the programs design in this study, the energy transformation ratio of all devices is provided in the Supplementary S5 as a reference for readers to estimate their performance.

Supplementary video related to this article can be found at <https://doi.org/10.1016/j.nanoen.2020.105241>

3. Conclusions

As demonstrated in this study, by leveraging the programming concept, it is very easy to achieve ~ kV level voltage output by a simple device without any material optimization. Even the same material, just like PTFE vs PTFE, still can generate high voltage, which is unachievable in conventional TENGs devices. However, it also faces some challenges and constraints. Theoretically, there is no upper limit for the energy output. The charge can have an infinite accumulation on the electrode. However, in real test, the breakdown, happening at 1 kV level, consumes the charge and limits the achievable voltage. One possible solution to improve this issue is to increase the dielectric layer thickness. As seen in the testing of Bennet doubler-based P-TENGs, a thicker dielectric layer can achieve a higher output voltage. But a thicker dielectric layer also reduces the capacitance between the electrodes, resulting in a higher inner impedance, which is undesirable for the energy harvesting purpose. A better solution is using high-k materials as the dielectric layer, which is a common method in the semiconductor industry to increase the capacitance and avoid the breakdown. We use PTFE and FEP films, which are optimal choices for conventional TENGs, in this study just because the inertial thinking inherited from conventional TENGs device. Since the P-TENGs is an alternative direction for designing the TENGs device, it also requires a completely different ideology. For P-TENGs, the surface treatment and the electronegativity is no longer the concern for material selection. Instead, we should find high-k materials, which are suitable for surface coating. Moreover, the breakdown also happens between the switch pads, which is highly affected by the actual shape of the switch pads. For example, tip shape is easier to have a breakdown while a blunter shape tends to have a breakdown at a higher voltage. This issue is quite practical and should be noticed in real device design and device preparation. There are several kinds of P-TENGs demonstrated in this study. We do not plan to compare the efficiency or performance of all these devices. The Bennet doubler and charge oscillator are used for different scenarios: one is for back and forth operation while another is for circular operations. Instead, we are more focused on demonstrating the endless possibilities of the programming concept. After mastering the three basic operations, G, T and O, everyone can design and realize his P-TENGs, maybe even better than the Bennet doubler and the charge oscillator.

4. Experimental section

Characterization: A programmable electrometer (Keithley model 6514) was used for the charges, and the output voltage was measured by an oscilloscope (Keysight, DSOX3034T) with an internal resistance 100 M Ω .

CRediT authorship contribution statement

Hao Wang: Methodology, Resources, Data curation, Formal analysis, Visualization, Writing - original draft, Writing - review & editing. **Jianxiong Zhu:** Methodology, Data curation, Formal analysis, Writing - original draft, Writing - review & editing. **Tianyi He:** Methodology, Writing - review & editing. **Zixuan Zhang:** Visualization, Writing - review & editing. **Chengkuo Lee:** Project administration, Funding acquisition, Writing - review & editing.

Declaration of competing interest

The authors declare that they have no known competing financial interests or personal relationships that could have appeared to influence the work reported in this paper.

Acknowledgment

H. Wang and J. Z. Zhu contributed equally to this work. This work has been conducted at NUS and is supported by the grants from the National Research Foundation Competitive research programme (NRF-CRP) ‘Energy Harvesting Solutions for Biosensors’ (R-263-000-A27-281), National Research Foundation Competitive research programme (NRF-CRP) ‘Piezoelectric Photonics Using CMOS Compatible AlN Technology for Enabling The Next Generation Photonics ICs and Nanosensors’ (R-263-000-C24-281), Shenzhen Basic Research Program and Guangdong Science and Technology Research Program (JCYJ20170818154035069; 2019A050503007), Faculty Research Committee (FRC) ‘Thermoelectric Power Generator (TEG) Based Self-Powered ECG Plaster - System Integration (Part 3)’ (R-263-000-B56-112) and HIFES Seed Funding ‘Hybrid Integration of Flexible Power Source and Pressure Sensors’ (R-263-501-012-133) at the National University of Singapore (NUS), Singapore; the A*STAR-NCBR research grant of ‘Chip-Scale MEMS Micro-Spectrometer for Monitoring Harsh Industrial Gases’ (R-263-000-C91-305) at the NUS, Singapore. Interests of intelligent property should refer to NUS.

Appendix A. Supplementary data

Supplementary data to this article can be found online at <https://doi.org/10.1016/j.nanoen.2020.105241>.

References

- [1] F.R. Fan, Z.Q. Tian, Z.L. Wang, Flexible triboelectric generator, *Nano Energy* 1 (2012) 328–334.
- [2] Z.L. Wang, Triboelectric nanogenerators as new energy technology for self-powered systems and as active mechanical and chemical sensors, *ACS Nano* 7 (11) (2013) 9533–9557.
- [3] Z.L. Wang, J. Chen, L. Lin, Progress in triboelectric nanogenerators as a new energy technology and self-powered sensors, *Energy Environ. Sci.* 8 (8) (2015) 2250–2282.
- [4] G. Zhu, Z.H. Lin, Q. Jing, P. Bai, C. Pan, Y. Yang, Y. Zhou, Z.L. Wang, Toward large-scale energy harvesting by a nanoparticle-enhanced triboelectric nanogenerator, *Nano Lett.* 13 (2) (2013) 847–853.
- [5] Z.L. Wang, On Maxwell’s displacement current for energy and sensors: the origin of nanogenerators, *Mater. Today* 20 (2) (2017) 74–82.
- [6] T. He, Q. Shi, H. Wang, F. Wen, T. Chen, J. Ouyang, C. Lee, Beyond energy harvesting-multi-functional triboelectric nanosensors on a textile, *Nano Energy* 57 (2019) 338–352.
- [7] Q. Shi, T. He, C. Lee, More than energy harvesting—Combining triboelectric nanogenerator and flexible electronics technology for enabling novel micro-/nano-systems, *Nano Energy* 57 (2019) 851–871.

- [8] C. Sun, Q. Shi, D. Hasan, M.S. Yazici, M. Zhu, Y. Ma, B. Dong, Y. Liu, C. Lee, Self-powered multifunctional monitoring system using hybrid integrated triboelectric nanogenerators and piezoelectric micro-sensors, *Nano Energy* 58 (2019) 612–623.
- [9] T. He, Z. Sun, Q. Shi, M. Zhu, D.V. Anaya, M. Xu, T. Chen, M.R. Yuce, A.V.Y. Thean, C. Lee, Self-powered glove-based intuitive interface for diversified control applications in real/cyber space, *Nano Energy* 58 (2019) 641–651.
- [10] M. Zhu, Q. Shi, T. He, Z. Yi, Y. Ma, B. Yang, T. Chen, C. Lee, Self-powered and self-functional cotton sock using piezoelectric and triboelectric hybrid mechanism for healthcare and sports monitoring, *ACS Nano* 13 (2) (2019) 1940–1952.
- [11] T. Chen, Q. Shi, M. Zhu, T. He, Z. Yang, H. Liu, L. Sun, L. Yang, C. Lee, Intuitive-augmented human-machine multidimensional nano-manipulation terminal using triboelectric stretchable strip sensors based on minimalist design, *Nano Energy* 60 (2019) 440–448.
- [12] Q. Shi, C. Qiu, T. He, F. Wu, M. Zhu, J.A. Dziuban, R. Walczak, M.R. Yuce, C. Lee, Triboelectric single-electrode-output control interface using patterned grid electrode, *Nano Energy* 60 (2019) 545–556.
- [13] Q. Shi, Z. Zhang, T. Chen, C. Lee, Minimalist and multi-functional human machine interface (HMI) using a flexible wearable triboelectric patch, *Nano Energy* 62 (2019) 355–366.
- [14] F.A. Hassani, R.P. Mogan, G.G. Gammad, H. Wang, S.C. Yen, N.V. Thakor, C. Lee, Toward self-control systems for neurogenic underactive bladder: a triboelectric nanogenerator sensor integrated with a bistable micro-actuator, *ACS Nano* 12 (4) (2018) 3487–3501.
- [15] H. Wang, H. Wu, D. Hasan, T. He, Q. Shi, C. Lee, Self-powered dual-mode amenity sensor based on the water–air triboelectric nanogenerator, *ACS Nano* 11 (10) (2017) 10337–10346.
- [16] L. Lin, Y. Xie, S. Wang, W. Wu, S. Niu, X. Wen, Z.L. Wang, Triboelectric active sensor array for self-powered static and dynamic pressure detection and tactile imaging, *ACS Nano* 7 (9) (2013) 8266–8274.
- [17] F.R. Fan, L. Lin, G. Zhu, W. Wu, R. Zhang, Z.L. Wang, Transparent triboelectric nanogenerators and self-powered pressure sensors based on micropatterned plastic films, *Nano Lett.* 12 (6) (2012) 3109–3114.
- [18] G. Zhu, W.Q. Yang, T. Zhang, Q. Jing, J. Chen, Y.S. Zhou, P. Bai, Z.L. Wang, Self-powered, ultrasensitive, flexible tactile sensors based on contact electrification, *Nano Lett.* 14 (6) (2014) 3208–3213.
- [19] Y. Yang, H. Zhang, Z.H. Lin, Y.S. Zhou, Q. Jing, Y. Su, J. Yang, J. Chen, C. Hu, Z. L. Wang, Human skin based triboelectric nanogenerators for harvesting biomechanical energy and as self-powered active tactile sensor system, *ACS Nano* 7 (10) (2013) 9213–9222.
- [20] B. Meng, W. Tang, Z.H. Too, X. Zhang, M. Han, W. Liu, H. Zhang, A transparent single-friction-surface triboelectric generator and self-powered touch sensor, *Energy Environ. Sci.* 6 (11) (2013) 3235–3240.
- [21] Y. Yang, H. Zhang, X. Zhong, F. Yi, R. Yu, Y. Zhang, Z.L. Wang, Electret film-enhanced triboelectric nanogenerator matrix for self-powered instantaneous tactile imaging, *ACS Appl. Mater. Interfaces* 6 (5) (2014) 3680–3688.
- [22] R.K. Gupta, Q. Shi, L. Dhakar, T. Wang, C.H. Heng, C. Lee, Broadband energy harvester using non-linear polymer spring and electromagnetic/triboelectric hybrid mechanism, *Sci. Rep.* 7 (2017) 41396.
- [23] W. Yang, J. Chen, X. Wen, Q. Jing, J. Yang, Y. Su, G. Zhu, W. Wu, Z.L. Wang, Triboelectrification based motion sensor for human-machine interfacing, *ACS Appl. Mater. Interfaces* 6 (10) (2014) 7479–7484.
- [24] L. Zhang, F. Xue, W. Du, C. Han, C. Zhang, Z. Wang, Transparent paper-based triboelectric nanogenerator as a page mark and anti-theft sensor, *Nano Res.* 7 (8) (2014) 1215–1223.
- [25] P. Bai, G. Zhu, Q. Jing, J. Yang, J. Chen, Y. Su, J. Ma, G. Zhang, Z.L. Wang, Membrane-based self-powered triboelectric sensors for pressure change detection and its uses in security surveillance and healthcare monitoring, *Adv. Funct. Mater.* 24 (37) (2014) 5807–5813.
- [26] Tianyi He, Hao Wang, Jiahui Wang, Xi Tian, Feng Wen, Qiongfeng Shi, S. John, Ho, and Chengkuo Lee, Self-sustainable wearable textile nano-energy nano-system (NENS) for next-generation healthcare applications, *Adv. Sci.* (2019), 1901437.
- [27] Qiongfeng Shi, Chengkuo Lee, Self-powered bio-inspired spider-net-coding interface using single-electrode triboelectric nanogenerator, *Adv. Sci.* 6 (15) (2019) 1900617.
- [28] Qiongfeng Shi, Zixuan Zhang, Tao Chen, Chengkuo Lee, Minimalist and multi-functional human machine interface (HMI) using A flexible wearable triboelectric patch, *Nano Energy* 62 (2019) 355–366.
- [29] Qiongfeng Shi, Chunkai Qiu, Tianyi He, Fan Wu, Minglu Zhu, Jan A. Dziuban, Rafal Walczak, Mehmet Rasit Yuce, Chengkuo Lee, Triboelectric single-electrode-output control interface using patterned grid electrode, *Nano Energy* 60 (2019) 545–556.
- [30] Sanghoon Lee, Hao Wang, Wendy Yen Xian Peh, Tianyi He, Shih-Cheng Yen, V. Nitish, Thakor, and Chengkuo Lee, Mechano-neuromodulation of autonomic pelvic nerve for underactive bladder: a triboelectric neurostimulator integrated with flexible neural clip interface, *Nano Energy* 60 (2019) 449–456.
- [31] Tao Chen, Qiongfeng Shi, Minglu Zhu, Tianyi He, Zhan Yang, Huicong Liu, Lining Sun, Lei Yang, Chengkuo Lee, Intuitive-augmented human-machine multidimensional nano-manipulation terminal using triboelectric stretchable strip sensors based on minimalist design, *Nano Energy* 60 (2019) 440–448.
- [32] Tianyi He, Zhongda Sun, Qiongfeng Shi, Minglu Zhu, David Vera Anaya, Mengya Xu, Tao Chen, Mehmet R. Yuce, Aaron Voon-Yew Thean, Chengkuo Lee, Self-powered glove-based intuitive interface for diversified control applications in real/cyber space, *Nano Energy* 58 (2019) 641–651.
- [33] Hao Wang, Han Wu, Dihan Hasan, Tianyi He, Qiongfeng Shi, Chengkuo Lee, Self-powered dual-mode amenity sensor based on the water–air triboelectric nanogenerator, *ACS Nano* 11 (10) (2017) 10337–10346.
- [34] Hao Wang, Giorgia Pastorin, Chengkuo Lee, Toward self-powered wearable adhesive skin patch with bendable microneedle array for transdermal drug delivery, *Adv. Sci.* (Wiley). 3 (9) (2016) 1500441.
- [35] N. Cui, L. Gu, Y. Lei, J. Liu, Y. Qin, X. Ma, Y. Hao, Z.L. Wang, Dynamic behavior of the triboelectric charges and structural optimization of the friction layer for a triboelectric nanogenerator, *ACS Nano* 10 (6) (2016) 6131–6138.
- [36] S. Niu, S. Wang, Y. Liu, Y.S. Zhou, L. Lin, Y. Hu, K.C. Pradel, Z.L. Wang, A theoretical study of grating structured triboelectric nanogenerators, *Energy Environ. Sci.* 7 (7) (2014) 2339–2349.
- [37] J. Peng, S.D. Kang, G.J. Snyder, Optimization principles and the figure of merit for triboelectric generators, *Sci. Adv.* 3 (12) (2017), eaap8576.
- [38] Cheng, X., Tang, W., Song, Y., Chen, H., Zhang, H. and Wang, Z.L., Power management and effective energy storage of pulsed output from triboelectric nanogenerator. *Nano Energy*, 61, p. 517–532.
- [39] H. Chen, Y. Song, X. Cheng, H. Zhang, Self-powered electronic skin based on the triboelectric generator, *Nano Energy* 56 (2019) 252–268.
- [40] H.J. Yoon, D.H. Kim, W. Seung, U. Khan, T.Y. Kim, T. Kim, S.W. Kim, 3D-printed biomimetic-villus structure with maximized surface area for triboelectric nanogenerator and dust filter, *Nano Energy* 63 (2019) 103857.
- [41] H. Oh, S.S. Kwak, B. Kim, E. Han, G.H. Lim, S.W. Kim, B. Lim, Highly conductive ferroelectric cellulose composite papers for efficient triboelectric nanogenerators, *Adv. Funct. Mater.* 29 (37) (2019) 1904066.
- [42] R. Hinchet, H.J. Yoon, H. Ryu, M.K. Kim, E.K. Choi, D.S. Kim, S.W. Kim, Transcutaneous ultrasound energy harvesting using capacitive triboelectric technology, *Science* 365 (6452) (2019) 491–494.
- [43] V.T. Bui, Q. Zhou, J.N. Kim, J.H. Oh, K.W. Han, H.S. Choi, S.W. Kim, I.K. Oh, Treefrog toe pad-inspired micropatterning for high-power triboelectric nanogenerator, *Adv. Funct. Mater.* 29 (28) (2019) 1901638.
- [44] J. Shao, D. Liu, M. Willatzen, Z.L. Wang, Three-dimensional modeling of alternating current triboelectric nanogenerator in the linear sliding mode, *Appl. Phys. Rev.* 7 (1) (2020), 011405.
- [45] X. Chen, L. Gao, J. Chen, S. Lu, H. Zhou, T. Wang, A. Wang, Z. Zhang, S. Guo, X. Mu, Z.L. Wang, A chaotic pendulum triboelectric-electromagnetic hybridized nanogenerator for wave energy scavenging and self-powered wireless sensing system, *Nano Energy* 69 (2020) 104440.
- [46] C. Zhang, L. Zhou, P. Cheng, X. Yin, D. Liu, X. Li, H. Guo, Z.L. Wang, J. Wang, Surface charge density of triboelectric nanogenerators: theoretical boundary and optimization methodology, *Appl. Mater. Today* 18 (2020) 100496.
- [47] W. Wang, A. Yu, X. Liu, Y. Zhang, Y. Zhu, Y. Lei, M. Jia, J. Zhai, Z.L. Wang, Large-scale fabrication of robust textile triboelectric nanogenerators, *Nano Energy* (2020) 104605.
- [48] J. Wang, Y. Li, Z. Xie, Y. Xu, J. Zhou, T. Cheng, H. Zhao, Z.L. Wang, Cylindrical direct-current triboelectric nanogenerator with constant output current, *Adv. Energy Mater.* (2020) 1904227.
- [49] Y. Ding, Y. Shi, J. Nie, Z. Ren, S. Li, F. Wang, J. Tian, X. Chen, Z.L. Wang, Thermochromic triboelectric nanogenerator enabling direct visualization of temperature change during operation, *Chem. Eng. J.* (2020) 124369.
- [50] Z. Xie, Z. Zeng, Y. Wang, W. Yang, Y. Xu, X. Lu, T. Cheng, H. Zhao, Z.L. Wang, Novel sweep-type triboelectric nanogenerator utilizing single free-wheel for random triggering motion energy harvesting and driver habits monitoring, *Nano Energy* 68 (2020) 104360.
- [51] Z. Lin, B. Zhang, H. Zou, Z. Wu, H. Guo, Y. Zhang, J. Yang, Z.L. Wang, Rationally designed rotation triboelectric nanogenerators with much extended lifetime and durability, *Nano Energy* 68 (2020) 104378.
- [52] G. Yao, L. Xu, X. Cheng, Y. Li, X. Huang, W. Guo, S. Liu, Z.L. Wang, H. Wu, Bioinspired triboelectric nanogenerators as self-powered electronic skin for robotic tactile sensing, *Adv. Funct. Mater.* 30 (6) (2020) 1907312.
- [53] J. Wang, C. Meng, Q. Gu, M.C. Tseng, S.T. Tang, H.S. Kwok, J. Cheng, Y. Zi, Normally transparent tribo-induced smart window, *ACS Nano* 14 (3) (2020) 3630–3639.
- [54] Y. Liu, L. Wang, L. Zhao, K. Yao, Z. Xie, Y. Zi, X. Yu, Thin, skin-integrated, stretchable triboelectric nanogenerators for tactile sensing, *Adv. Electron. Mater.* 6 (1) (2020) 1901174.
- [55] J. Wang, H. Wang, X. Li, Y. Zi, Self-powered electrowetting optical switch driven by a triboelectric nanogenerator for wireless sensing, *Nano Energy* 66 (2019) 104140.
- [56] C. Wu, H. Tetik, J. Cheng, W. Ding, H. Guo, X. Tao, N. Zhou, Y. Zi, Z. Wu, H. Wu, D. Lin, Electrohydrodynamic jet printing driven by a triboelectric nanogenerator, *Adv. Funct. Mater.* 29 (22) (2019) 1901102.
- [57] G. Xu, X. Li, X. Xia, J. Fu, W. Ding, Y. Zi, On the force and energy conversion in triboelectric nanogenerators, *Nano Energy* 59 (2019) 154–161.
- [58] F. Chen, Y. Wu, Z. Ding, X. Xia, S. Li, H. Zheng, C. Diao, G. Yue, Y. Zi, A novel triboelectric nanogenerator based on electrospun polyvinylidene fluoride nanofibers for effective acoustic energy harvesting and self-powered multifunctional sensing, *Nano Energy* 56 (2019) 241–251.
- [59] X. Li, G. Xu, X. Xia, J. Fu, L. Huang, Y. Zi, Standardization of triboelectric nanogenerators: progress and perspectives, *Nano Energy* 56 (2019) 40–55.
- [60] X. Li, T.H. Lau, D. Guan, Y. Zi, A universal method for quantitative analysis of triboelectric nanogenerators, *J. Mater. Chem. A* 7 (33) (2019) 19485–19494.
- [61] H. Qin, G. Cheng, Y. Zi, G. Gu, B. Zhang, W. Shang, F. Yang, J. Yang, Z. Du, Z. L. Wang, High energy storage efficiency triboelectric nanogenerators with unidirectional switches and passive power management circuits, *Adv. Funct. Mater.* 28 (51) (2018) 1805216.
- [62] X. He, H. Zou, Z. Geng, X. Wang, W. Ding, F. Hu, Y. Zi, C. Xu, S.L. Zhang, H. Yu, M. Xu, A hierarchically nanostructured cellulose fiber-based triboelectric

- nanogenerator for self-powered healthcare products, *Adv. Funct. Mater.* 28 (45) (2018) 1805540.
- [63] M.C. Bernier, A. Li, L. Winalski, Y. Zi, Y. Li, C. Caillet, P. Newton, Z.L. Wang, F. M. Fernández, Triboelectric nanogenerator (TEENG) mass spectrometry of falsified antimalarials, *Rapid Commun. Mass Spectrom.* 32 (18) (2018) 1585–1590.
- [64] J. Cheng, W. Ding, Y. Zi, Y. Lu, L. Ji, F. Liu, C. Wu, Z.L. Wang, Triboelectric microplasma powered by mechanical stimuli, *Nat. Commun.* 9 (1) (2018) 1–11.
- [65] C. Xu, A.C. Wang, H. Zou, B. Zhang, C. Zhang, Y. Zi, L. Pan, P. Wang, P. Feng, Z. Lin, Z.L. Wang, Raising the working temperature of a triboelectric nanogenerator by quenching down electron thermionic emission in contact-electrification, *Adv. Mater.* 30 (38) (2018) 1803968.
- [66] Y. Zi, C. Wu, W. Ding, X. Wang, Y. Dai, J. Cheng, J. Wang, Z. Wang, Z.L. Wang, Field Emission of electrons powered by a triboelectric nanogenerator, *Adv. Funct. Mater.* 28 (21) (2018) 1800610.
- [67] J. Nie, X. Chen, Z.L. Wang, Electrically responsive materials and devices directly driven by the high voltage of triboelectric nanogenerators, *Adv. Funct. Mater.* 29 (41) (2019) 1806351.
- [68] J. Wang, Y. Zi, S. Li, X. Chen, High-voltage applications of the triboelectric nanogenerator—opportunities brought by the unique energy technology, *MRS Energy Sustain.* 6 (2020).
- [69] G. Liu, S. Xu, Y. Liu, Y. Gao, T. Tong, Y. Qi, C. Zhang, Flexible drug release device powered by triboelectric nanogenerator, *Adv. Funct. Mater.* (2020) 1909886.
- [70] L. Zhang, B. Meng, Y. Xia, Z. Deng, H. Dai, P. Hagedorn, Z. Peng, L. Wang, Galloping triboelectric nanogenerator for energy harvesting under low wind speed, *Nano Energy* (2020) 104477.
- [71] A.C. Wang, B. Zhang, C. Xu, H. Zou, Z. Lin, Z.L. Wang, Unraveling temperature-dependent contact electrification between sliding-mode triboelectric pairs, *Adv. Funct. Mater.* (2020) 1909384.
- [72] S. Li, Y. Fan, H. Chen, J. Nie, Y. Liang, X. Tao, J. Zhang, X. Chen, E. Fu, Z.L. Wang, Manipulating the triboelectric surface charge density of polymers by low-energy helium ion irradiation/implantation, *Energy Environ. Sci.* 13 (3) (2020) 896–907.
- [73] Z. Zhao, Q. Huang, C. Yan, Y. Liu, X. Zeng, X. Wei, Y. Hu, Z. Zheng, Machine-washable and breathable pressure sensors based on triboelectric nanogenerators enabled by textile technologies, *Nano Energy* 70 (2020) 104528.
- [74] H. Liu, Y. Feng, J. Shao, Y. Chen, Z.L. Wang, H. Li, X. Chen, Z. Bian, Self-cleaning Triboelectric nanogenerator based on TiO₂ photocatalysis, *Nano Energy* (2020) 104499.
- [75] X. Liang, T. Jiang, G. Liu, Y. Feng, C. Zhang, Z.L. Wang, Spherical triboelectric nanogenerator integrated with power management module for harvesting multidirectional water wave energy, *Energy Environ. Sci.* 13 (1) (2020) 277–285.
- [76] H. Huo, F. Liu, Y. Luo, Q. Gu, Y. Liu, Z. Wang, R. Chen, L. Ji, Y. Lu, R. Yao, J. Cheng, Triboelectric nanogenerators for electro-assisted cell printing, *Nano Energy* 67 (2020) 104150.
- [77] C. Chen, L. Chen, Z. Wu, H. Guo, W. Yu, Z. Du, Z.L. Wang, 3D double-faced interlock fabric triboelectric nanogenerator for bio-motion energy harvesting and as self-powered stretching and 3D tactile sensors, *Mater. Today* 32 (2020) 84–93.
- [78] W. Harmon, D. Bamgboje, H. Guo, T. Hu, Z.L. Wang, Self-driven power management system for triboelectric nanogenerators, *Nano Energy* (2020) 104642.
- [79] S. Chun, C. Pang, S.B. Cho, Triboelectric energy: a micropillar-assisted versatile strategy for highly sensitive and efficient triboelectric energy generation under in-plane stimuli, *Adv. Mater.* 32 (2) (2020) 2070009.
- [80] J. Liao, Y. Zou, D. Jiang, Z. Liu, X. Qu, Z. Li, R. Liu, Y. Fan, B. Shi, Z. Li, L. Zheng, Nestable arched triboelectric nanogenerator for large deflection biomechanical sensing and energy harvesting, *Nano Energy* 69 (2020) 104417.
- [81] Y. Tang, H. Zhou, X. Sun, N. Diao, J. Wang, B. Zhang, C. Qin, E. Liang, Y. Mao, Triboelectric touch-free screen sensor for noncontact gesture recognizing, *Adv. Funct. Mater.* 30 (5) (2020) 1907893.
- [82] S. Yan, K. Dong, J. Lu, W. Song, R. Xiao, Amphiphobic triboelectric nanogenerators based on silica enhanced thermoplastic polymeric nanofiber membranes, *Nanoscale* 12 (7) (2020) 4527–4536.
- [83] S. Li, D. Liu, Z. Zhao, L. Zhou, X. Yin, X. Li, Y. Gao, C. Zhang, Q. Zhang, J. Wang, Z. L. Wang, A fully self-powered vibration monitoring system driven by dual-mode triboelectric nanogenerators, *ACS Nano* 14 (2) (2020) 2475–2482.
- [84] X. Cui, Y. Zhang, G. Hu, L. Zhang, Y. Zhang, Dynamical charge transfer model for high surface charge density triboelectric nanogenerators, *Nano Energy* 70 (2020) 104513.
- [85] A. Ghaffarinejad, Y. Lu, R. Hinchet, D. Galayko, J.Y. Hasani, P. Basset, July. Bennet's charge doubler boosting triboelectric kinetic energy harvesters, *J. Phys. Conf. Ser.* 1052 (No. 1) (2018), p. 012027. IOP Publishing.
- [86] A. Ghaffarinejad, J.Y. Hasani, R. Hinchet, Y. Lu, H. Zhang, A. Karami, D. Galayko, S.W. Kim, P. Basset, A conditioning circuit with exponential enhancement of output energy for triboelectric nanogenerator, *Nano Energy* 51 (2018) 173–184.
- [87] H. Zhang, Y. Lu, A. Ghaffarinejad, P. Basset, Progressive contact-separate triboelectric nanogenerator based on conductive polyurethane foam regulated with a Bennet doubler conditioning circuit, *Nano Energy* 51 (2018) 10–18.
- [88] W. Liu, Z. Wang, G. Wang, G. Liu, J. Chen, X. Pu, Y. Xi, X. Wang, H. Guo, C. Hu, Z. L. Wang, Integrated charge excitation triboelectric nanogenerator, *Nat. Commun.* 10 (1) (2019) 1426.
- [89] L. Cheng, Q. Xu, Y. Zheng, X. Jia, Y. Qin, A self-improving triboelectric nanogenerator with improved charge density and increased charge accumulation speed, *Nat. Commun.* 9 (1) (2018) 3773.
- [90] L. Xu, T.Z. Bu, X.D. Yang, C. Zhang, Z.L. Wang, Ultrahigh charge density realized by charge pumping at ambient conditions for triboelectric nanogenerators, *Nano Energy* 49 (2018) 625–633.
- [91] B.D. Truong, C.P. Le, E. Halvorsen, Analysis of MEMS electrostatic energy harvesters electrically configured as voltage multipliers, *AEU-Int. J. Electron. Commun.* 107 (2019) 125–136.
- [92] A. Ghaffarinejad, J.Y. Hasani, D. Galayko, P. Basset, Superior performance of half-wave to full-wave rectifier as a power conditioning circuit for triboelectric nanogenerators: application to contact-separation and sliding mode TENG, *Nano Energy* 66 (2019) 104137.
- [93] J. Luo, Z.L. Wang, Recent advances in triboelectric nanogenerator based self-charging power systems, *Energy Storage Mater.* 23 (2019) 617–628.
- [94] M.B. Ouanes, H. Samaali, D. Galayko, P. Basset, F. Najjar, A new type of triboelectric nanogenerator with self-actuated series-to-parallel electrical interface based on self-synchronized mechanical switches for exponential charge accumulation in a capacitor, *Nano Energy* 62 (2019) 465–474.
- [95] X. Xia, H. Wang, P. Basset, Y. Zhu, Y. Zi, An inductor-free output multiplier for power promotion and management of triboelectric nanogenerators toward self-powered systems, *ACS Appl. Mater. Interfaces* 12 (5) (2020) 5892–5900.
- [96] A. Ghaffarinejad, J.Y. Hasani, Modeling of triboelectric charge accumulation dynamics at the metal–insulator interface for variable capacitive structures: application to triboelectric nanogenerators, *Appl. Phys. A* 125 (4) (2019) 259.
- [97] Y. Liu, W. Liu, Z. Wang, W. He, Q. Tang, Y. Xi, X. Wang, H. Guo, C. Hu, Quantifying contact status and the air-breakdown model of charge-excitation triboelectric nanogenerators to maximize charge density, *Nat. Commun.* 11 (1) (2020) 1–8.
- [98] Q. Tang, X. Pu, Q. Zeng, H. Yang, J. Li, Y. Wu, H. Guo, Z. Huang, C. Hu, A strategy to promote efficiency and durability for sliding energy harvesting by designing alternating magnetic stripe arrays in triboelectric nanogenerator, *Nano Energy* 66 (2019) 104087.
- [99] W. Liu, Z. Wang, G. Wang, G. Liu, J. Chen, X. Pu, Y. Xi, X. Wang, H. Guo, C. Hu, Z. L. Wang, Integrated charge excitation triboelectric nanogenerator, *Nat. Commun.* 10 (1) (2019) 1–9.



Dr Hao Wang Received his B.Eng. degree in School of Opto-electronic Information from University of Electronic Science and Technology of China in 2010, and Ph.D. degree from the National University of Singapore in 2016. After that, he was a Research Fellow of ECE, NUS, from 2016 to 2019. He is currently an associate Professor in Shenzhen Institutes of Advanced Technology (SIAT), China. His research interests are focused on nanoneedle devices for transdermal drug delivery, flexible and wearable electronics, energy harvesting and electrical neural stimulations.



Dr. Jianxiang Zhu received his B.Eng. degree in Electrical and Automation Engineering from the Hubei University of Technology in 2006. After that, he got his Master's degree from the University of Science and Technology of China and Ph.D. from the University of Missouri Columbia in 2015. He is currently a Research Fellow of ECE, NUS. His research interests are focused on MEMS zero-power sensor, wearable flexible sensor, and gas sensor.



Dr. Tianyi He received her B.Eng. degree from the School of Microelectronics and Solid-state Electronics at the University of Electronic Science and Technology of China (UESTC), Chengdu, China, in 2016, and her Ph.D. degree from Department of Electrical and Computer Engineering at the National University of Singapore in 2020. She is currently a Research Fellow in the Dept. of ECE, NUS. Her research interests are focused on wearable energy harvesters and self-powered sensors.



Zixuan Zhang received his B.Eng. degree from the School of Mechanical and Electrical Engineering at the University of Electronic Science and Technology of China (UESTC), Chengdu, China, in 2018. He is now a Master student in the Department of Electrical and Computer Engineering, National University of Singapore. His research interests include self-powered wearable sensors, energy harvesters and triboelectric nanogenerators.



Prof. Chengkuo Lee received his Ph.D. degree in Precision Engineering from The University of Tokyo in 1996. Currently, he is the director of the Center for Intelligent Sensors and MEMS at the National University of Singapore, Singapore. He was a Senior Member of IEEE. He has contributed to more than 300 peer-reviewed international journal articles. His ORCID is 0000-0002-8886-3649.